Sub-picosecond Raman spectrometer for time-resolved studies of structural dynamics in heme proteins

5 AUTHORS, INCLUDING:

Sergei G Kruglik
Pierre and Marie Curie University - Paris 6
99 PUBLICATIONS **921** CITATIONS

SEE PROFILE

Jean-Christophe Lambry
École Polytechnique
78 PUBLICATIONS **2,290** CITATIONS

SEE PROFILE

Jean-Louis Martin
Ecole Polytechnique & French Institute of H…
236 PUBLICATIONS **7,319** CITATIONS

SEE PROFILE

Marten H Vos
École Polytechnique
142 PUBLICATIONS **3,665** CITATIONS

SEE PROFILE

Journal of RAMAN SPECTROSCOPY

Sub-picosecond Raman spectrometer for time-resolved studies of structural dynamics in heme proteins

Sergei G. Kruglik,[a,b] Jean-Christophe Lambry,[b] Jean-Louis Martin,[b] Marten H. Vos[b] and Michel Negrerie[b]*

We describe a pump–probe Raman spectrometer based on a femtosecond Ti : sapphire laser, an optical parametric generator and two optical parametric amplifiers for time-resolved studies, with emphasis on the structural dynamics in heme proteins. The system provides a 100-fs pump pulse tunable in the range 500–600 nm and a transform-limited sub-picosecond probe pulse tunable in the range 390–450 nm. The spectrometer has spectral (25 cm^{-1}) and temporal ($\sim$ 0.7 ps) resolutions which constitute an effective compromise for identifying transient heme protein species and for following their structural evolution by spontaneous Raman scattering in the time range 0.5 ps to 2 ns. This apparatus was applied to time-resolved studies of a broad range of heme proteins, monitoring the primary dynamics of photoinduced heme coordination state and structural changes, its interaction with protein side-chains and diatomic gaseous ligands, as well as heme vibrational cooling. The treatment of transient Raman spectra is described in detail, and the advantages and shortcomings of spontaneous resonance Raman spectroscopy for ultrafast heme proteins studies are discussed. We demonstrate the efficiency of the constructed spectrometer by measuring Raman spectra in the sub-picosecond and picosecond time ranges for the oxygen-storage heme protein myoglobin and for the oxygen-sensor heme protein FixLH in interaction with the diatomic gaseous ligands CO, NO, and O_2. Copyright © 2010 John Wiley & Sons, Ltd.

Supporting information may be found in the online version of this article.

Introduction

For several decades, time-resolved optical spectroscopies based upon the pump–probe methodology are used for studying numerous molecular systems. In this perspective, picosecond and later femtosecond transient absorption (TA) spectroscopy, either in the visible[1–6] or in the infrared (IR)[7–11] range, became a unique tool in studying the structural dynamics of heme proteins. After absorption of the excitation pulse (pump) by the heme, several processes are triggered and the evolution of the system is recorded by the delayed probe pulse. The diverse events following the photoexcitation are both photophysical and chemical/structural: dissociation of an axial ligand from the heme iron, change of its spin state, formation and decay of excited states, vibrational heating/cooling, as well as heme and protein structural relaxations. All these events take place within the first 10 ps and may influence each other, so that their identification and kinetic analysis cannot be achieved unambiguously by a single spectroscopic technique. For example, the identification of a transient four-coordinate heme in a NO-receptor was indirectly made by analyzing the kinetics of the absorption spectral components, but a direct unequivocal proof was lacking[5] and the geminate rebinding of NO and O_2 in oxygen-sensor proteins can occur with a 5 ps time constant, similar to that of heme excited state decay.[6] Thus, for understanding the primary molecular mechanisms, it is essential to separate the contributions from the often simultaneous events mentioned above. For this purpose, time-resolved resonance Raman (TR^3) spectroscopy is a valuable tool because of its resonance selectivity

and its rich spectral information due to intrinsic high resolution, which allow discrimination of various short-lived transient species in an evolving system. For example, the photodissociation of one axial ligand from a six-coordinate heme results in the motion of the central iron out of the heme plane toward a five-coordinate domed structure,[12–25] leading to a change in Raman activity for some modes, in particular the Fe–His stretch (215–235 cm^{-1}).[26] Pronounced wavenumber shifts of porphyrin marker bands also occur as a result of heme coordination and spin-state changes.[27] Therefore, TR^3 spectroscopy is known as a direct, structure-sensitive tool for investigating the processes of energy relaxation and structural perturbations within heme proteins and their model compounds.[12–34]

While pump–probe TR^3 experiments in the nanosecond and longer time range can be achieved by electronic synchronization between two pulsed ultrafast laser sources,[30] faster processes require a different methodology.[35] Early TR^3 spectrometers were based on dye lasers with 4 ps[36] or 1 ps[14] time resolution,

---

* Correspondence to: Michel Negrerie, Laboratoire d'Optique et Biosciences, Ecole Polytechnique, INSERM, 91128 Palaiseau, France.
E-mail: michel.negrerie@polytechnique.fr

a Laboratoire Acides Nucléiques et Biophotonique, Université Pierre & Marie Curie, 75252 Paris, France

b Laboratoire d'Optique et Biosciences (LOB), Ecole Polytechnique, INSERM, 91128 Palaiseau, France

the latter having a repetition rate of 30 Hz and a diode array detection. This method has provided valuable information on myoglobin (Mb) and hemoglobin[14,16,17] but required very long acquisition times and the use of rapidly degrading dyes such as coumarin. Another system[37] based on two picosecond dye lasers synchronously pumped by a mode-locked master Nd : YAG laser yielded a 5-ps time jitter and 1-MHz repetition rate, parameters which are not suitable for ultrafast studies of heme proteins. In the last decade, a large number of TR³ studies[18,19,31–33] were performed with a system based on picosecond Ti : sapphire laser[38] having a temporal resolution of about 2 ps. The tunability of the pump and probe pulses was generally achieved by means of a water continuum generation,[38] by a Raman shifter,[39,40] or by optical parametric generation/amplification (OPG/OPA).[38,41] A Kerr-gated TR³ spectrometer with about 1 ps resolution based on OPG/OPA has been reported,[41–43] which allowed wide tuning of both pump and probe pulses by frequency mixing. In this design, the probe pulse was not transform-limited and yielded bandwidths between 25 and ∼50 cm⁻¹ depending on the probing wavelength because of spectral filtering during the OPA process. In another OPG/OPA system,[38] pulses with a bandwidth of >50 cm⁻¹ have been reported that could be used in a pump but not in a probe channel of a TR³ spectrometer. We note, nevertherless, a TR³ experiment utilizing 250-fs pulses for probing very broad Raman bands of water,[44] so that the ultrafast dynamics of hydrated electron relaxation could be measured. However, the spectral line width of 160 cm⁻¹ in this experiment is far too broad for heme proteins studies.

Ultrafast vibrational spectroscopy is also performed by means of several nonlinear Raman techniques[45–52] which have already shown their rich potential, and here we just briefly overview some of their shortcomings with respect to the studies of heme protein dynamics.

In femtosecond stimulated Raman spectroscopy (FSRS), a narrowband 3-ps pulse providing Raman excitation is superimposed on a femtosecond probe pulse stimulating the Raman emission.[45] In FSRS, the spectral line shape of the gain signal strongly depends upon the position of Raman excitation wavelength, upon the absorption profile of the transient species[46] and upon the pump–probe time delay.[47] Since the probed molecule does not discriminate between the two simultaneous pump and probe pulses, several nonlinear processes may occur,[46] which must be taken into account through rigorous analysis of the data.[46,48] The intensity of the major lines may considerably vary in FSRS as compared to their TR³ counterparts,[49] so that the interpretation becomes ambiguous, especially in the case of substantial spectral changes caused by heme structural rearrangements. The spectral width of the femtosecond stimulating broadband pulse determines the wavenumber range of Raman spectra[45] and the low wavenumber range (180–600 cm⁻¹) requires a stimulating pulse spectrum close to that of the Raman excitation. It is clear that the choice of particular technique strongly depends on the molecular system under study and the process to be probed: FSRS offers fluorescence rejection and femtosecond temporal resolution, which ensures, for example, the identification of intermediate states within 200 fs in the process of retinal isomerization[50] and β-carotene internal conversion,[49] whereas spontaneous TR³ is better suited for studies of heme structural dynamics.

Another four-wave mixing technique – coherent anti-Stokes (CARS)/Stokes Raman scattering – may also be used to probe ultrafast structural changes and vibrational dynamics.[51] The main problem of CARS in time-resolved studies of complex molecules

such as heme proteins resides in interference terms between the lines originating from different vibronic states and also with the nonresonant background, so that the CARS spectral profile is difficult to interpret. To extract the vibrational spectrum of the photoproduct of interest, an elaborate mathematical treatment of CARS spectra is required, which would contain many variable parameters in the case of heme proteins. Furthermore, in femtosecond time-resolved CARS, a delay is introduced between the pump pulses, so that the vibrational dynamics (wave packet) can be efficiently probed,[51,52] but not the coordination state as in heme–axial ligand interaction. We note that neither FSRS nor femtosecond-CARS studies on heme proteins have been reported so far.

Transient vibrational modes can also be measured by femtosecond coherence spectroscopy (FCS). This technique probes wave packet dynamics in a time window as oscillations, which are measured and converted into the wavenumber domain.[53] The detected wavenumber range is limited by the pulse duration on the high wavenumber side and by the intensity of the signal and the width of time window on the low wavenumber side. The calculated wavenumbers are assigned to a transient species within the entire probed time interval (usually 1–4 ps) during which electronic and/or structural changes take place. In other words, in FCS the time resolution cannot be smaller than the window used for performing the time to wavenumber conversion, and the increase of time resolution by probing a narrower time window decreases the ability to detect the low wavenumber vibrations. In FCS applied to the study of heme protein–ligand interaction,[54] the time window was limited to ∼4 ps because of the damping of the wave packet and the decrease of signal intensity. Nevertheless, this technique, although being indirect due to necessity of the time to wavenumber conversion, is efficient in measuring very low wavenumber modes (50–200 cm⁻¹)[55] not readily accessible in TR³ due to strong Rayleigh scattering.

The above considerations show that further exploration of the use of sub-picosecond transform-limited Raman probe pulse is required in order to achieve the best possible time resolution for spontaneous Raman spectroscopy, while keeping spectral resolution sufficient for interpretation of transient spectra related to primary structural changes in heme proteins. We have developed a pump–probe TR³ spectrometer based on a femtosecond 1-kHz Ti : sapphire laser and OPG/OPA system, combined with a set of specially designed narrowband interference filters, which provides an efficient compromise between temporal (∼0.7 ps) and spectral (∼25 cm⁻¹) resolutions and which has been approbated in studies of various heme proteins.[20–25] In this paper, we describe in detail the constructed spectrometer and the procedure of TR³ data treatment and we present results of TR³ study on the oxygen-storage Mb and the oxygen-sensor heme protein FixL in interaction with diatomic gaseous ligands in sub-picosecond and picosecond time ranges.

Experimental

Laser source system

The laser source system (Fig. 1) comprises a home-built femtosecond Ti : sapphire oscillator[56] pumped by a solid-state diode-pumped laser (Spectra Physics, Millenia) producing 50-fs pulses with a repetition rate of 80 MHz and an average power of about 190 mW. The seed pulse from this oscillator was stretched, amplified, and then compressed in a regenerative amplifier (Spectra
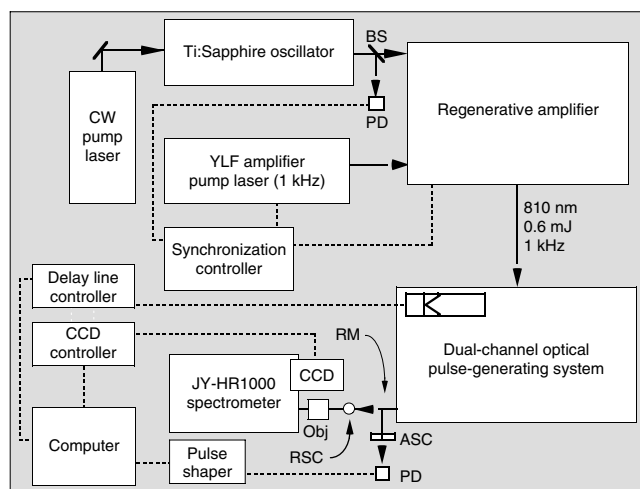
Figure 1. Overview of the system for sub-picosecond Raman measurements. The solid line between blocks is the laser beam, while the dashed line represents an electronic signal. PD, photodiode; BS, beam-splitter; Obj, objective; RM, retractable mirror; ASC, absorption sample cell; RSC, Raman sample cell. The specially designed dual-channel optical pulse-generating system is detailed in Fig. 2.

Physics, Spitfire) pumped by a Q-switched frequency-doubled (527 nm) Nd : YLF laser (Spectra Physics, Merlin) with a repetition rate of 1 kHz. The synchronization between the pump laser and the oscillator was performed with a Synchronization and Delay Generator (Spectra Physics) which provided adjustable delayed trigger signals for switching the Pockels cells in the regenerative amplifier. The output radiation at 810 nm from the regenerative amplifier after the pulse compression stage had pulse energy of ∼0.6 mJ with pulse duration of about 50 fs. This radiation was used to feed the home-built dual-channel optical system based on optical parametric generator (OPG) and two noncollinear optical parametric amplifiers (NOPA) for the simultaneous generation of pump and probe tunable pulses, which is detailed in Fig. 2.

Dual-channel optical pulse-generating system

The 810-nm beam from regenerative amplifier was first separated in two parts by an 80/20 beam splitter: the weaker part was used to generate the seed pulses in the OPG, whereas the stronger part allowed their amplification in two NOPAs. In both arms, the second harmonic ($\lambda = 405$ nm) was produced in 0.5-mm β-barium borate (BBO) crystals (SHG1, SHG2). In the generating arm, this radiation was used to pump an OPG utilizing a 2-mm BBO crystal. Within the cone of parametric emission, two different wavelengths were selected by means of circular pinholes, one for the pump pulse in 550–600 nm range (which can easily be extended to even longer wavelengths) and another in 820–900 nm range (note that the range 780–820 nm is covered by the master laser) for the Raman probe. The choice of particular pump and probe wavelengths is dictated by the position of absorption bands of the heme protein under study, and therefore by the narrowband filter wavelength for the probe channel. It should be noted that, if a pump wavelength in the range 500–545 nm is required, the optical scheme must be slightly modified to incorporate either two OPGs or two white-light continuum generators, since it is difficult to obtain stable and efficient parametric generation from a single BBO crystal in the whole wavelength range 500–900 nm. We also note that utilization of a strong parametric radiation from the OPG together with selecting pineholes, instead of white-light continuum generation, provides more energy at the chosen wavelengths (at the expense of sligthly decreased temporal resolution).

The amplification in the pump and probe channels was symmetrically designed and utilized two 2-mm BBO crystals (NOPA1, NOPA2), which were pumped by the 405-nm radiation split in two beams (50/50). The focusing of the 405-nm beam was performed by means of spherical mirrors (M1, M2) with a focal length of 250 mm. The temporal overlaps between the seed and the pump pulses in NOPAs were ensured by tunable delay-line stages (DL1, DL2).

The duration of the pump pulse after amplification in NOPA2 was ∼100 fs as chirp-compensating prisms were not employed.
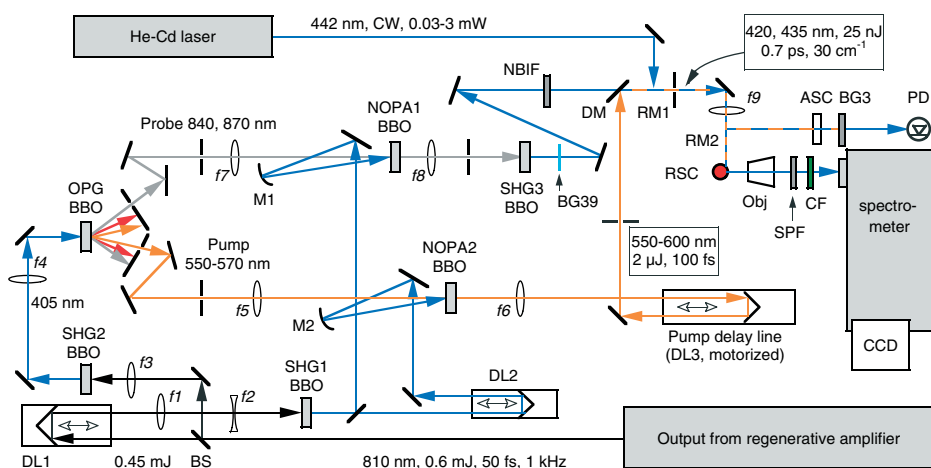

Figure 2. Dual-channel pulse-generating system. The wavelength selection after the optical parametric generation is achieved by tuning the crystal and moving the pinholes. The delay line DL3 is equipped with a three-mirror corner cube. A mirror is placed under the Raman sample cell to vertically direct the beams up to the cell. BS, beam-splitter; DL1, DL2, manually adjustable delay line stages; DL3, computer-controlled motorized delay line stage; SHG1, SHG2, SHG3, second harmonic generators; OPG, optical parametric generator; M1, M2, concave mirrors; NOPA1, NOPA2, noncollinear optical parametric amplifiers; NBIF, narrowband interference filter; DM, dichroic mirror; RM1, RM2, retractable mirrors; RSC, Raman sample cell; Obj, objective; SPF, short wavelength pass filter; CF, long-path cutoff filter; ASC, absorption sample cell; PD, photodiode. The focal lengths (cm) are respectively from f1 to f9: 40, −10, 40, 30, 25, 20, 25, 10, and 10. The width of the crystals is given in the text.

The pump pulse energy was reduced by the appropriate pinholes to the range 1.5–2.5 µJ in the sample cell. In all our heme protein studies, the pump wavelength actually employed ranged from 550 to 580 nm.[20–25] The excitation in the Q-bands of hemoproteins (around 570 nm) allows effective photodissociation of the diatomic axial ligand from the heme, without large excess of energy, contrary to the excitation in the Soret band (around 400 nm), which causes substantial heating. Because the maxima of Q-band absorption depend strongly upon the nature of heme protein and diatomic ligand, one must have the capability of fine-tuning the pump wavelength.

In the probe channel, near-IR radiation either at 840 or 870 nm was selected for all experiments on heme proteins[20–25] by an appropriate pinhole position and diameter. Initial alignment of the probe channel was facilitated by the insertion of a retractable broadband filter (λ_{center} = 840 or 870 nm, 10 nm FWHM, Corion) placed behind the OPG. The IR light was directed through a set of mirrors, pinholes, and a lens to be amplified in the NOPA1, and then frequency-doubled in a 4-mm BBO crystal (SHG3) to produce Raman probe beam at either 420 or 435 nm. The remaining near-IR radiation was blocked by the colored filter (BG39, Schott) and the Raman probe light passed through a specially designed (Barr Associates) narrowband interference filter (NBIF), which represents a crucial part of the TR^3 spectrometer as it solely determines the temporal and spectral resolutions of the whole system. The parameters of NIBF are the following: 0.45 nm FWHM and ~0.60 nm full spectral width at 10% of maximum; the transmission is ~76% at maximum (either 420 or 435 nm) and below 10^{-3} at 2.5 nm apart from central wavelength. The Raman probe pulse energy was in the range 20–40 nJ in the sample cell for both probe wavelengths employed. It should be noted that each Raman probe wavelength requires its own NBIF and matched cutoff filter (CF). Any wavelength within the Soret band maximum of the heme protein of interest (~390–450 nm) can, in principle, be selected, provided that the appropriate filters set is designed and utilized.

The optical time delay (Δt) between the pump and the probe pulses was controlled by a motorized translation stage (DL3, Newport M–ILS250PP) equipped with a three-mirror retroreflector (Melles Griot). The stage allowed measuring Raman spectra at time delays up to 1.8 ns, and this range can be further extended up to several nanoseconds by an additional mirrors set.

Sample compartment and detection system

Spectra were recorded using a 90° light-collection geometry with the excitation from the bottom of a spinning Raman sample cell (Fig. 3, insert). The pump and probe beams were collinearly superimposed by a dichroic mirror, focused by a spherical lens with f = 10 cm, and directed vertically by a folding mirror (Fig. 3), entering from the bottom of the cell in order to travel parallel to the meniscus film formed by the rotation of the sample. The focused probe beam size was 40–50 µm in the sample cell, while that of the pump beam was 130–150 µm effectively overlapping the probe beam spot. Polarizations of both beams were set parallel to each other since protein reorientation is negligible in the picosecond time scale.

The sample (heme protein in buffer solution) was placed in the cylindrical UV-quartz spinning cell (Hellma Ref 540-135; internal diameter 18 mm), which was held in a home-built spinning mechanism containing two ball bearings (Fig. 3). The liquid sample created a thin film on the internal cell surface; the film thickness
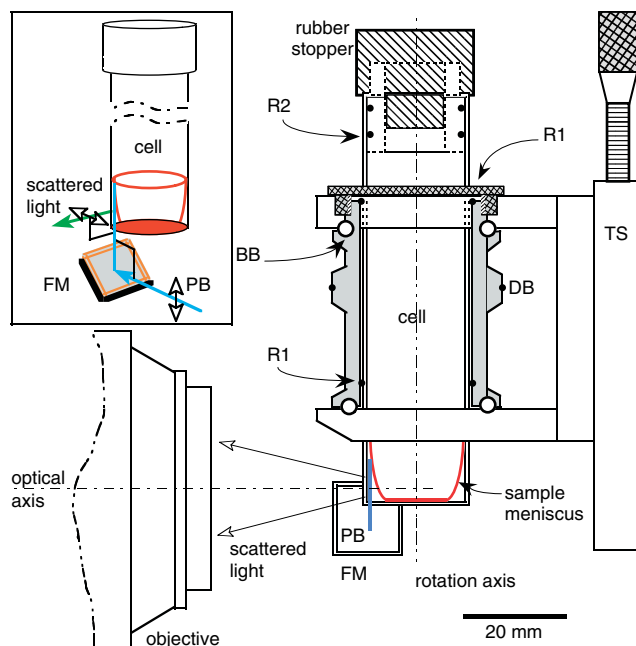

Figure 3. Section of the spinning cell compartment in a vertical plane defined by the rotation and optical axis. The inset shows in perspective the geometric arrangement of the beams, with the doubled-sized arrows indicating their polarization. The internal diameter and height of the cell are, respectively, 18 and 75 mm. The distance between the cell and the entrance face of the objective is 35 mm. The optical axis is located 2.5–3 mm from the internal bottom of the cell. The thickness of the sample film is controlled by adjusting the rotational speed of the cell. The small electric motor that rotates the cell by means of a rubber drive belt (DB) is attached to the holder and thus is moved jointly with the cell when adjusting the translation stage (TS). BB, ball bearing; FM, folding mirror to position the beam vertically through the bottom of cell; PB, probe beam overlapped with the pump beam; R1, rubber O-rings for maintaining the cell; R2, rubber O-rings for gas tightness of the cell.

depended on the rotation speed, which was adjustable up to 1000 rpm, depending upon the sample, for maximizing the signal and minimizing its photodegradation. Since the laser beams were positioned just inside the sample film layer at a distance of less than 50 µm from the inner cell surface, such an experimental arrangement allowed us to use a sample volume as low as 50 µl. The solution was routinely vacuumed and the gas phase was exchanged through the rubber stopper using a needle connected to the gas train. The large volume of the gas phase (~20 ml) allowed a complete equilibration between the protein and the diatomic ligands (CO, NO, or O_2).

Alternatively, the sample can also be placed in a five-window, 1-cm standard quartz cuvette containing a small magnetic stirrer ensuring the exchange of the illuminated volume. However, this configuration requires a much larger amount of sample and provides less optimal conditions for gas equilibration, and the speed of sample movement through the illuminated area can be insufficient for certain heme proteins.

Raman scattering was efficiently collected by a camera lens (Leica, Noctilux-M, f = −50 mm, $f/1$) onto a 1-m spectrograph (Jobin-Yvon, HR1000) equipped with either 1200 or 600 groves mm^{-1} grating and whose slit width was set to 0.4 mm for sub-picosecond TR^3 studies. The Raman spectra were recorded by a liquid-nitrogen-cooled CCD (Roper Scientific, Spec-10:100B) detector. Parasitic background due to strong pump light scattering was largely suppressed by two short-pass filters (SPF, Melles Griot).
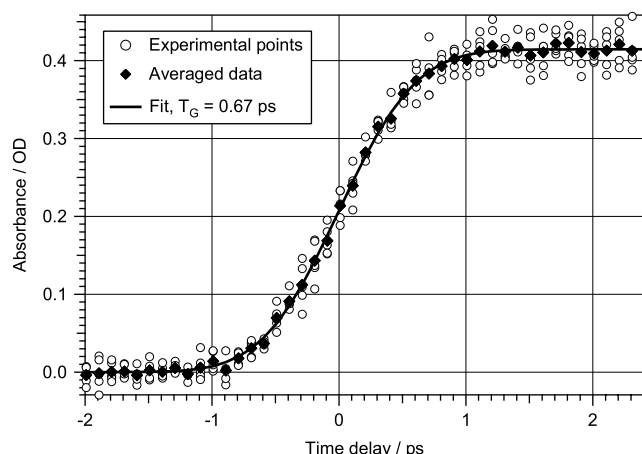
Figure 4. Determination of the zero-delay time point and instrumental response function via photoinduced absorption changes in copper(II)-octaethylporphyrin in toluene (2-mm path length cell). The pump and probe pulses were those used in TR^3 experiment without any change in energy, wavelength, or optical path. Open markers are the measured data points (five scans), filled markers are the averaged data points, and the solid curve represents the fit using Eqn (1).

Rayleigh scattering was rejected by a custom-designed long-pass sharp CF (Barr Associates), which was fabricated as a matching pair to the corresponding NBIF. The filter had a transmission of 10^{-4} at the Rayleigh wavelength and 80% at 3.5 nm above the Rayleigh wavelength, corresponding to a Raman shift of 200 cm^{-1} for a probe at 420 nm; these values were, respectively, 2.5 nm and ~130 cm^{-1} for a Raman probe at 435 nm. TR^3 spectra were accumulated by repetitive averaging 20- to 30-s exposures, with typical accumulation time ranging from 5 to 15 min and up to 60 min in the case of very weak Raman signal on the fluorescent background. For polarization measurements, a thin-film polarizer could be inserted just after the Leica objective lens (Obj) in combination with a quartz scrambler placed on the entrance slit.

Continuous-wave Raman measurements

We always recorded the continuous wave (cw) Raman spectra of the same sample with the same apparatus to unambiguously identify the transient vibrational bands. The steady-state resonance Raman measurements of all heme proteins studied were carried out using a He–Cd laser (Liconix) with cw excitation at 441.6 nm with a power in the range 0.03–3 mW at the sample position. For this purpose, the cw beam was directed to the sample compartment by means of a retractable mirror (RM1; Fig. 2). Importantly, cw Raman spectra were recorded with the spinning cell in the same position as for TR^3 measurements and with the same spectrometer, optics, and detection system. Resolution of the cw Raman spectra was ~5 cm^{-1}.

Spectrometer calibration and specifications

Determination of the zero-delay time point has to be performed before each TR^3 experiment; a typical kinetics is shown in Fig. 4. The measurement is based on the photoinduced absorption changes in copper(II)-octhaethylporphyrin (CuOEP) in toluene, employing the ultrafast internal conversion of photoexcited CuOEP into the tripdoublet-quartet state manifold which strongly absorbs within the 420–435 nm range and whose absorption in the ground state in this spectral region is only very minor.[57] The solution

of CuOEP in toluene was placed in a quartz 2-mm standard cell (Hellma, 110-QS2, ASC in Fig. 2) and continuously moved in a specially designed cell holder perpendicularly to the laser beam. The superimposed pump and probe laser beams were directed into this absorption cell by positioning a retractable mirror (RM2) just before the Raman sample cell. Absorption of the probe beam was measured with a photodiode connected to a pulse shaper and an analog to digital (AD) converter. A set of color filters (BG3 Schott) was inserted after the absorption cell to suppress the pump beam intensity. Importantly, in this absorption measurement the mutual orientation of the pump and probe beams, their duration, energies, and wavelengths, as well as the focusing conditions, were exactly the same as used in further TR^3 experiments.

Assuming Gaussian temporal pulses shape, the following formula was used for fitting the absorption change as a function of time delay t:

$$\Delta A(t) = C \int_0^\infty \exp\left(-\frac{(x-t)^2}{T_G{}^2}\right) dx \qquad (1)$$

The instrumental response function represents the cross correlation between the 100-fs pump and the probe pulse, mainly defined by the width and shape of the longer probe pulse. The fitting procedure allows the determination of the point $\Delta t = 0$ (at half maximum of the fitted rise of absorption) with an accuracy better than 0.2 ps. In Fig. 4, the fitting function has a half-width of $T_G = 0.67$ ps, which effectively defines the temporal resolution. Having recorded more than 100 kinetics, we found that the instrumental time response function always lay within the range $T_G = 0.65 \pm 0.06$ ps, corresponding to a Gaussian FWHM of ~1.1 ps (FWHM $= 2\sqrt{\ln 2} \times T_G$). According to our experience, the value of half-width T_G (~0.7 ps) characterizes time-resolved pump–probe experiments more accurately than FWHM (~1.1 ps) and corresponds to the experimental rise. Indeed, at time delay of −1 ps between pump and probe pulses, we have never observed any photoinduced changes for heme proteins (Fig. 6), although the primary photoreaction of axial ligand dissociation is extremely fast (<100 fs). Note that this value of T_G is an upper-limit estimate since the response of CuOEP to photoexcitation was assumed to be instantaneous, which is not exactly the case,[57] so that the instrumental response time may actually be shorter by up to ~0.1 ps.

From the viewpoint of temporal resolution, one of the main advantages of the present time-resolved Raman spectrometer compared to picosecond laser systems[30–33,38,40] consists in employing 100-fs pump pulses *versus* ≥2 ps pump pulses. As a result, the transient photoproduct can be initiated almost instantaneously, thus avoiding an undesirable saturation effect during the action of the pump pulse and allowing disentanglement of vibrational relaxation (which widens certain bands in transient spectra) from structural effects in the time range of 0.5–5 ps. Moreover, the probe pulse duration that determines the overall spectrometer response function is also shorter for the system based on femtosecond Ti : sapphire laser and NBIF. The sub-picosecond resolution of the present spectrometer is achieved by proper deconvolution of the instrument response function, and is supported by the absence of photoinduced changes in transient Raman spectra routinely taken at time delay $\Delta t = -1$ ps (Fig 6(b); see also Figs 5 and 7 of Ref. [22]). The spectral bandwidth of Raman lines was measured to be ~25 cm^{-1} (FWHM) with excitation at both 420 and 435 nm. This value is solely determined by the design of the NBIF employed.
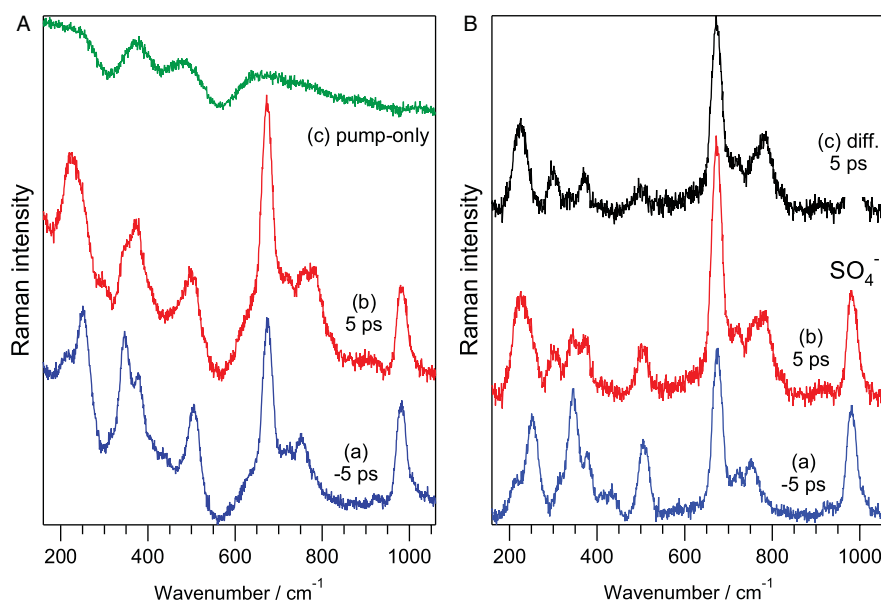
Figure 5. Illustration of TR³ spectra treatment for Mb–CO, as described in detail in the text. Experimental conditions: accumulation time $= 10$ min for each spectrum, $\lambda_{pump} = 570$ nm, $\lambda_{probe} = 435$ nm. Panel (A): raw experimental spectra recorded at time delay Δt between pump and probe pulses of -5 ps (a), $+5$ ps (b), and without the probe pulse (c). Panel (B): normalized processed spectra at -5 ps (a), $+5$ ps (b), and their difference spectrum (c). Vertical offsets between spectra are arbitrary and introduced for clarity.

The Raman wavenumber calibration was carried out by using Kr and Xe spectral lamps (Oriel) with an absolute accuracy of ± 2 cm^{-1} and a relative accuracy better than 1 cm^{-1}. Raman intensity normalization was performed using the 980 cm^{-1} stretching mode of sulfate (0.2–0.5 M) added to the buffer solution (ammonium or sodium sulfate was used, depending upon the stability of the proteins to both salts, to avoid precipitation). When a high salt concentration could not be used, the normalization and subtraction coefficients were obtained from an additional calibration procedure using a sulfate buffer solution containing Mb-CO, as described below.

This spectrometer employed a laser source working at the repetition rate of 1 kHz. The fast motion of the sample in the spinning cell, together with the large surface of exchange between the gas phase and the sample film, was sufficient to avoid photoproduct accumulation due to possible binding processes longer than 1 ms. To verify the absence of long-lived pump-induced spectral changes, as well as the absence of probe-induced changes, the pump–probe spectrum taken at time delay $\Delta t = -5$ ps was routinely compared with the probe-only spectrum and with the cw spectrum; no essential differences were found, except for the difference in spectral resolution between TR³ and cw spectra.

Sample preparation

The solution of ferric horse heart Mb was prepared from the lyophilized powder (Sigma Chemical) without further purification in phosphate buffer, pH 7.4. Wild-type FixL was overexpressed and purified as described[58] and prepared in 50 mM HEPES buffer, pH 8.0. The protein samples (60–150 µl, at a concentration of 200 µM) were placed in the cylindrical UV-quartz spinning cell closed with a rubber stopper, and degassed by four successive cycles of vacuum and purging with argon (Air Liquide, 99.999%). The sample was reduced by addition of 10 µl of degassed sodium dithionite in the cell ($Na_2S_2O_4$) to obtain 2 mM final concentration. For preparing

CO and NO-liganded heme proteins, argon was replaced with pure CO or with NO (10% in N_2) directly introduced into the cell after vacuuming, both at a pressure of ~ 1.2 bar. The volume of the gas phase was at least 100-fold more than that of the protein solution. For preparing oxygenated samples, Mb was reduced with sodium dithionite whereas the O_2-sensor FixL was reduced with sodium ascorbate (5 mM final concentration). Then, air or pure O_2 was introduced into the cell and the samples were used immediately. The optical density (OD) was between 0.1 and 0.25 in the Q-bands for an optical path length of 1 mm. The procedure was controled in parallel in a 1-mm absorption cell (Fig. S1, Supporting Information) and the state of the sample was immediately verified after Raman experiment by transferring the solution in a 1-mm path length cell and measuring the absorption in the Q-bands. In the case of repeated Raman measurements of O_2-liganded proteins, the sample was exchanged for a fresh one every 10 min (Mb) or 5 min (FixL). All measurements were performed at ambient temperature.

Treatment of TR³ spectra

The TR³ spectra of heme proteins recorded at positive time delays always contain contributions from both the photoinduced and the ground-state species. There are two aspects of this behavior. First, the pump intensity is usually chosen in such a way that only a fraction of the ground-state molecules are photoexcited in order to minimize saturation effects. This is especially important when the pump pulse duration is longer than the excited state decay because of the probability of repetitive photon absorption by the same molecule in the ground state within the same pump pulse. In contrast, in the case of a short 100-fs pulse, the pump intensity may be chosen sufficiently strong to increase the photodissociation yield: in all our studies,[20–25] 30–60% of molecules (depending on the protein) were usually photoexcited by the 100-fs pulse, as determined experimentally on the basis of ground-state contribution in the transient spectra. It should be noted that, although NOPA allows obtaining a pulse duration as
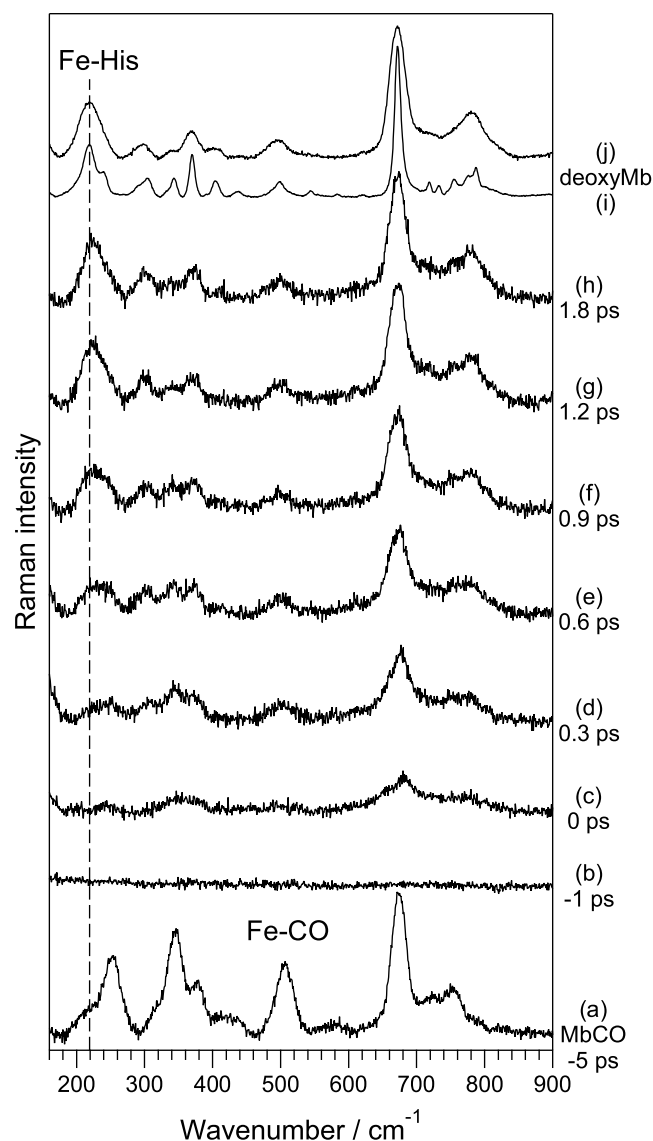
Figure 6. TR^3 spectra of Mb–CO in the low wavenumber range. Experimental conditions: accumulation time = 20 min for each spectrum, λ_{pump} = 570 nm, λ_{probe} = 435 nm. Spectra are the initial ground-state Mb–CO (a) and difference spectra (b–h) corresponding to the Mb photoproduct at $\Delta t = -1$ ps (b), 0 ps (c), 0.3 ps (d), 0.6 ps (e), 0.9 ps (f), 1.2 ps (g), and 1.8 ps (h). Traces (i) and (j) are Raman spectra of deoxy–Mb obtained with cw (i) and sub-picosecond (j) excitations. The dashed line indicates the position of the ν(Fe–His) stretch at 219 cm^{-1} for deoxy–Mb. TR^3 spectra from 2 to 100 ps are presented in Fig. S2.

Figure 7. TR^3 spectra in the high wavenumber range of the Mb–CO complex (λ_{pump} = 570 nm, λ_{probe} = 435 nm, accumulation time =10 min). Spectrum (a) represents the ground-state Mb–CO, while the difference spectra (b–e) correspond to the Mb photoproduct at $\Delta t = 0.3$ ps (b), 0.7 ps (c), 1 ps (d), and 10 ps (e).

short as ∼15 fs, we have chosen to use longer 100-fs pump pulses in order to reduce undesirable nonlinear optical effects.

Second, Raman scattering from both the initial ground-state and the photoproduct species experiences resonance enhancement since the heme protein absorption bands are rather broad. Even though the Raman probe wavelength is in resonance with the photoproduct absorption maximum, it is not possible to suppress completely the resonance Raman signal from the initial ground-state species because its absorption maximum is too close to that of the photoproduct and their respective absorptions partially overlap.

Therefore, the main goal of TR^3 spectra treatment is to extract the pure photoproduct contribution from the overall spectrum.
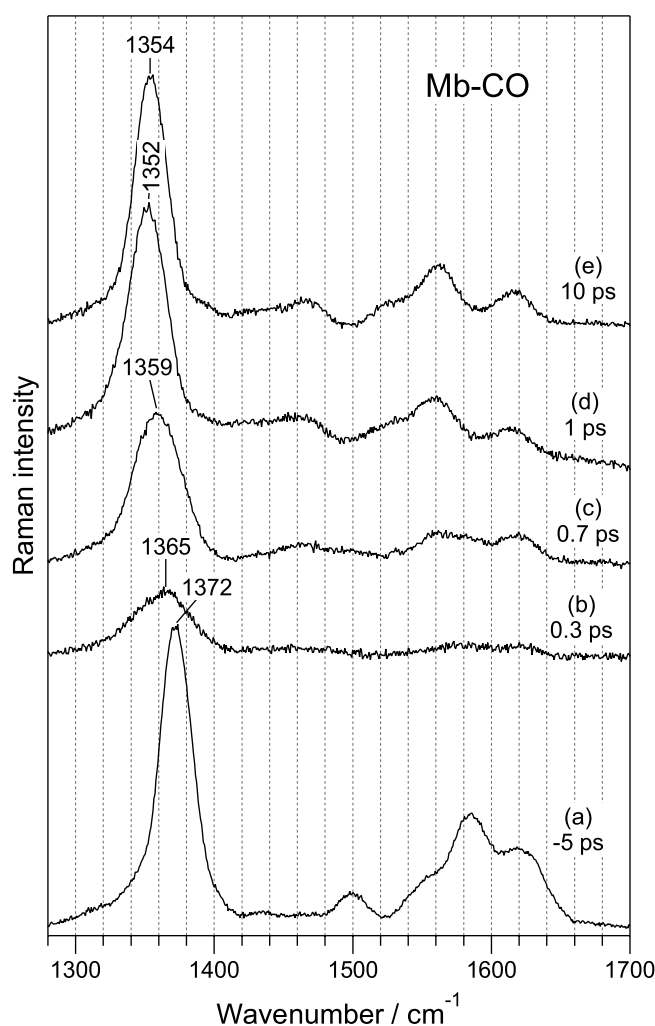
Figure 5 shows in detail an example of this treatment procedure for Mb–CO at $\Delta t = +5$ ps which comprises the following steps.

1. Raman spectra were recorded with both pump and probe beams present in the sample, at $\Delta t = -5$ ps (spectrum a) and +5 ps (spectrum b). We emphasize that spectra in Fig. 5(A) are the original data, presented as obtained in the experiment. The former spectrum contains pure ground-state contribution; the latter one is the linear mixture of the ground-state and the photoproduct species.

2. The spectrum without the probe beam was recorded (pump only; Fig. 5(A), spectrum (c)) with all other conditions being the same. This spectrum contains the residual contribution from the parasitic background signal due to strong pump pulse.

3. Spectrum (c) was subtracted (1:1) from spectra (a) and (b) effectively correcting the measured TR^3 spectra for both CCD dark current and pump-induced background.

4. The resulting spectra were divided by the transmission curve of the optical elements employed in the collection path (Obj + SPF + CF + spectrometer), and the remaining slowly varying background (in the range 160–560 cm^{-1} in this particular

case) was eliminated by subtracting a cubic spline function manually matched with the baseline of spectra. The origin of such a background is usually either the tail of the Rayleigh scattering and/or fluorescence from aromatic residues or from impurities in a sample solution. The contribution from the quartz cell was not generally observed because of the 90° light-collection geometry and the proper choice of the height of the entrance slit.

5. The resulting spectra at $\Delta t = -5$ ps (Fig. 5(B), spectrum (a)) and 5 ps (Fig. 5(B), spectrum (b)) were normalized on the internal Raman intensity standard, the 980 cm^{-1} line of $SO_4{}^{2-}$ stretching. This normalization procedure compensates for (1) power fluctuations of the probe beam with time, (2) change of light reabsorption in the photoproduct state, and (3) change of scattering volume (the depth of penetration of the probe beam) in the presence of the pump beam.

6. Lastly, in order to obtain a pure photoproduct spectrum, removing the contribution from nonphotolyzed molecules, a subtraction procedure was implemented, expressed in the general form as:

$$\text{Product spectrum } (\Delta t) = \text{normalized spectrum } (\Delta t) - [K(\Delta t)$$
$$\times \text{ normalized spectrum}(-5 \text{ ps})] \quad (2)$$

where the time-dependent factor $K(\Delta t)$ indicates the amount of the ground-state contribution. In the particular case of Fig. 5(B), we have:

$$\text{spectrum (c)} = \text{spectrum (b)} - 0.4 \times \text{spectrum (a)} \quad (3)$$

Hence, the difference Raman spectrum at $\Delta t = 5$ ps (Fig. 5(B), spectrum (c)) represents the pure scattering from the transient Mb species after CO photodissociation. The value of $K(\Delta t)$ can be determined with good accuracy ($\pm 10\%$) provided the photoproduct spectrum contains new bands and/or bands that are shifted substantially with respect to their ground-state counterparts. In practice, the value of $K(\Delta t)$ should be varied until negative features corresponding to the characteristic bands of the ground-state species appear in the difference Raman spectrum.

We note that, in principle, the most usual procedure for obtaining the photoproduct spectrum should contain a weighted subtraction of a probe-only spectrum,[59] and not the pump–probe spectrum at $\Delta t = -5$ ps. However, one must always verify before any kinetic measurement that the probe-only spectrum corrected on dark current is equal the spectrum at $\Delta t = -5$ ps (after pump-only spectrum subtraction), in order to confirm the absence of sample degradation due to the pump and accumulation of a long-lived photoproduct species. Thus, the use of a pump–probe spectrum at $\Delta t = -5$ ps is purely instrumental, as it gives the same final result, but also has an important advantage: one can easily verify the presence of photoinduced changes by 1 : 1 subtraction of pump–probe spectra at any particular Δt and -5 ps, since the pump-only and dark-current contributions are effectively cancelled during such a subtraction.

Results and Discussion

Primary structural changes of the heme in myoglobin after CO dissociation

We demonstrated the capabilities of the constructed TR^3 spectrometer by studying the primary structural changes of the heme in Mb in interaction with the gaseous ligand CO through temporal evolution of the photoproduct Raman spectra (Figs 6 and 7). The optical density of the Mb–CO sample was ~2 for 1-mm optical path at 435 nm (Raman probe) and ~0.25 in the Q-bands (570-nm pump). Figure 6 presents the initial temporal evolution, up to 1.8 ps after CO dissociation, of spectra in the low wavenumber range 160–900 cm^{-1} containing the Fe–His stretch at ~220 cm^{-1}. We also recorded the Raman spectra in the time range 2–100 ps (Fig. S2, Supporting Information), which are in agreement with already reported spectra taken with 2.3 ps time resolution.[18,31] Raman spectra of deoxy myoglobin in cw and TR^3 configurations (5- and 25-cm^{-1} spectral resolution, respectively) are compared (Fig. 6(i) and (j)), and the wavenumbers and assignements of the prominent Raman bands are presented in Table 1. It is evident that the lines appear broadened in the TR^3 spectrum compared to those in the cw spectrum, as expected for the 25 cm^{-1} probe pulse. Nevertheless, TR^3 spectra contain most features required for structural analysis; so the spectral resolution of the present spectrometer is sufficient to study heme protein structural dynamics. For example, we can observe the wavenumber shift of the ν(Fe–His) stretch from

Table 1. Wavenumbers (cm^{-1}) of Raman bands in spectra of Mb–CO, Mb photoproduct after CO photodissociation, and deoxy–Mb (data from Figs 6 and S2)

Mode assignment[60]	Mb–CO TR^3 (−5 ps)	Mb photoproduct TR^3 (+1.8 ps)	Mb photoproduct TR^3 (+100 ps)	Deoxy–Mb TR^3 (−5 ps)	Deoxy–Mb cw Raman
ν(Fe–His)	−	222	221	219	219
ν_9	253	(b)	(b)	(b)	239
γ_7	−	300	300	298	304
ν_8	345	(a)	(a)	342	343
δ(C–C–C)	379	370	370	369	370
γ_{12}	−	498	498	496	499
ν(Fe–CO)	507	−	−	−	−
ν_7	673	672	672	672	672
ν_{15}	752	(b)	(b)	(b)	755
ν_{47}	−	780 (c)	780 (c)	780 (c)	776
ν_6	(a)	780 (c)	780 (c)	780 (c)	787

(a) Insufficient accuracy and wavenumber resolution for determination of the mode position; (b) weak contribution to the contour: band is buried under strong neighboring band; (c) substantial contribution to the contour: wavenumber resolution is insufficient to resolve the overlapping bands.

225 ($\Delta t = +0.9$ ps) to 221 cm^{-1} ($\Delta t = +100$ ps) and 219 cm^{-1} (deoxy–Mb), the mode which is directly related to the heme doming motion, together with the relative intensity changes of several Raman bands in the range 250–400 cm^{-1}.

Sub-picosecond temporal resolution ($T_G \approx 0.7$ ps) allows us to follow primary structural events during the very first moments after photoexcitation. Besides the wavenumber shift of ν(Fe–His) stretch, several other observations can be reported from spectra in Figs 6 and S2. The out-of-plane mode of pyrrole rings γ_{12} (496–499 cm^{-1}), which is active only for a domed heme,[60] appears at $\Delta t = +0.3$ ps and does not change in intensity at longer time delays, indicating that the Fe–CO bond cleavage occurs faster than 300 fs. At the same time, the intensities of the modes γ_7 (298–304 cm^{-1}) and $\delta_{(C\beta–C–C)}$ (370 cm^{-1}) evolve differently relative to each other. In the spectra at $\Delta t = +1.8$ ps (Fig. 6) and up to 100 ps (Fig. S2), the modes γ_7 and $\delta_{(C\beta–C–C)}$ have similar intensities, whereas in the deoxy spectra the $\delta_{(C\beta–C–C)}$ mode has a higher intensity (approximately two times) than the γ_7 mode. This observation suggests a structural perturbation of the heme,[61] which does not relax in picosecond time scale to stationary deoxy configuration, as observed at longer (microsecond) delays for hemoglobin.[30] Furthermore, the ν(Fe–His) intensity clearly increases more slowly than the ν_7 in-plane mode intensity. Indeed, the structural relaxation of the proximal His, as well as of the heme and its substituents, does not necessarily occur at the same rate.

In the high wavenumber range (1280–1700 cm^{-1}), the ultrafast spectral changes in the position, shape, and intensity of the in-plane marker band ν_4 are shown in Fig. 7. This mode constitutes a marker for heme coordination and oxidation states[27] and is also sensitive to vibrational relaxation.[22] The initial ν_4 band-shift from ~1372 cm^{-1} for Mb-CO to ~1365 cm^{-1} at $\Delta t = +0.3$ ps (Fig. 7) is caused by the change of coordination state of the heme iron after CO dissociation, followed by the creation of vibrationally hot five-coordinate species. Further, the ν_4 band evolution is quite peculiar: from $\Delta t = +0.3$ ps to 1 ps, the ν_4 band wavenumber of transient Mb shifts from 1365 to 1352 cm^{-1}, and then becomes centered at 1354 cm^{-1} at $\Delta t = +10$ ps (Fig. 7(e)). Such a complex time-dependent shift is due to intramolecular vibrational energy redistribution followed by intermolecular vibrational relaxation, whose accurate observation requires sub-picosecond resolution. This phenomenon was resolved for the first time for heme proteins and studied in detail previously for the heme protein cytochrome c using the present TR^3 spectrometer.[22] A similar alternating wavenumber shift has been previously reported[62] for the extensively studied C=C stretch at 1570 cm^{-1} of singlet excited $trans$-stilbene.[63]

Concerning ultrafast temporal evolution of Raman bands intensities, it is very important to note that the resonance Raman scattering intensity from the photoinduced transient species depends on both population of the photoproduct state and on Raman resonance enhancement, which is directly related to the absorption line shape.[64] For heme proteins, as for all metalloporphyrin compounds, the photoproduct absorption experiences substantial band-shifts and shape changes during the first few picoseconds after photoexcitation[57,64] and these changes are rather difficult to quantify; hence, the relationship between transient Raman intensities and photoproduct population is not straightforward. Therefore, in the majority of protein studies we used jointly femtosecond TA and sub-picosecond TR^3 spectroscopy to fully characterize the ultrafast heme protein dynamics.[21–25] TA spectroscopy is generally used to determine the rate constants associated with coordination and spin states, while TR^3 spec-

troscopy allows their identification and interpretation with respect to heme geometry and coordination, owing to its high spectral selectivity.

Primary processes in oxygen sensor FixLH after photodissociation of O$_2$, NO and CO

The conformation of the heme in sensor proteins depends upon the diatomic ligand bound to the heme and upon the structure of the protein as well, and its structural dynamics following ligand release can be studied by TR^3. Figure 8 presents the comparison of the TR^3 spectra of the heme transient of the oxygen storage-protein Mb with that of the oxygen-sensor FixL heme domain (FixLH) after the photodissociation of three diatomic ligands O$_2$, NO, and CO. The spectra of deoxy species provide a reference for the unliganded heme conformation. The low wavenumber spectrum of deoxy FixLH (Fig. 8(d), right panel) comprises the ν(Fe–His) stretch (~220 cm^{-1}); heme out-of-plane modes γ_7 (~293 cm^{-1}) and γ_{12} (~495 cm^{-1}); heme in-plane modes ν_8(~340 cm^{-1}), ν_7(~675 cm^{-1}), and ν_6(~795 cm^{-1}); and heme side-chain deformation modes $\delta_{(C–C–C)}$ (~408) cm^{-1} (mode assignments according to Refs [60, 65]).

Conspicuously, ν(Fe–His) is present in the spectra of Mb after dissociation of all three gaseous ligands (Fig. 8, left panel), indicating that full doming of the heme already occured at +1 ps in all three cases, as a consequence of bond cleavage and ligand migration. In contrast, in the case of FixLH a similar strong ν(Fe–His) band, and thus heme doming, occurs only for CO dissociation (Fig. 8(c), right panel). The absence of ν(Fe–His) stretch after O$_2$ dissociation at $\Delta t = +1$ ps (Fig. 8(a), right panel) indicates that heme doming does not occur, in agreement with O$_2$ trapping mechanism in FixLH[25] inducing ultrafast O$_2$ rebinding.[58] As for FixLH–NO, contrary to Mb–NO and much similarly to FixLH–O$_2$, only a week band at the position of ν(Fe–His) stretch is seen at +2 ps (Fig. 8(b), right), revealing that only a minor fraction of the heme experienced doming after NO dissociation. This finding is in agreement with an ultrafast NO recombination after photodissociation (5.3 ps for 62% of FixLH population).[58] Since in the case of FixLH–NO at $\Delta t = +2$ ps, the ν(Fe–His) area is about one-third of that of deoxy species, it could be assigned to the remaining 38% of FixLH population[58] to which photodissociated NO does not rebind in 5 ps, allowing heme doming, but with longer time constants (20 and 220 ps).[58] Thus, our data suggest that, after dissociation, CO is not trapped in the heme cavity, NO is only partially trapped, whereas O$_2$ is fully trapped.[25] This fully agrees with the behavior of the absorption spectrum after dissociation, which also depends upon the nature of the ligand[58] and appears much greatly shifted to that of bound species after O$_2$ than after NO dissociation, while it shows almost the shape of deoxy species spectrum after CO release.

The evolution of the heme modes γ_7, ν_8, and $\delta_{(C–C–C)}$ in the range 300–400 cm^{-1} also depends on the nature of the photodissociated ligand. In the case of the sensor FixLH, this vibrational pattern differs from that of deoxy FixLH (−5 ps, Fig. 8(d)) after dissociation of all three diatomics, albeit for CO this pattern is close to that of deoxy species. The heme has not yet relaxed to its deoxy state at +1 ps, but the effect is much more pronounced for NO and O$_2$, and these two ligands imposed a heme structure different from each other and from that of CO-liganded species. Even for Mb, the γ_7, ν_8, and $\delta_{(C–C–C)}$ pattern at +1 ps is different for both NO and O$_2$. The most strinking feature is the difference between NO- and O$_2$-dissociated FixL, revealing the difference in
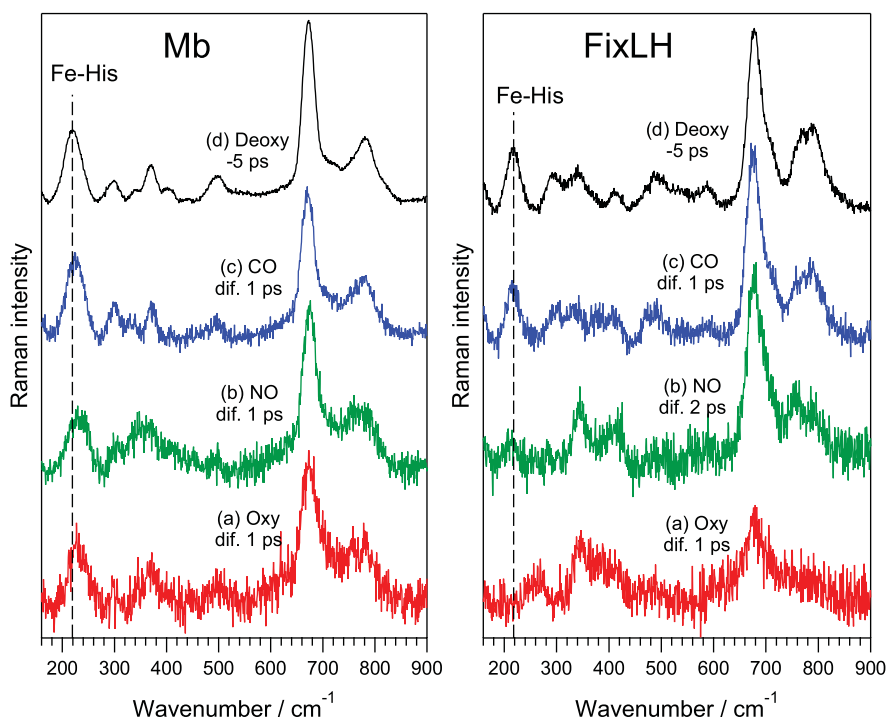
Figure 8. Comparison of transient difference Raman spectra taken at $\Delta t = 1$ ps (2 ps for FixLH–NO) in the low wavenumber range for Mb (left panel) and FixLH (right panel), for different gaseous axial ligands: O_2 (a); NO (b) and CO (c). Spectra (d) represent the unligated deoxy form of the respective heme protein recorded at $\Delta t = -5$ ps.

constraints exerted on the heme by these ligands, which depends upon the protein structure itself. This comparison of Mb and FixLH examplifies the ability of observing the very first steps of heme protein structural dynamics with a sub-picosecond Raman probe pulse.

Conclusions

We constructed a sub-picosecond TR^3 spectrometer with spectral resolution of 25 cm^{-1} (and ~1 cm^{-1} accuracy for band shift detection) and temporal resolution $T_G \approx 0.7$ ps, with an accuracy for the zero-delay time position better than 0.2 ps. The use of a transform-limited sub-picosecond Raman probe pulse together with a femtosecond pump pulse ($T_{pump} \approx 100$ fs) was proven effective in TR^3 measurements of primary structural changes in a broad range of heme proteins, including the following:

- Photodissociation and ultrafast rebinding of the internal ligand methionine in ferrous cytochrome c[20,22];
- Ultrafast vibrational relaxation and interaction of nitric oxide with cytochrome c[21,22];
- Identification of the transient four-coordinate heme in bacterial cytochrome c'[24] and the H93G Mb mutant[23];
- Oxygen trapping in the heme pocket of the bacterial oxygen sensor FixLH.[25]

We presented a comparative measurement of two different heme proteins interacting with the diatomics O_2, NO, and CO. In the case of ferrous Mb, we have shown the existence of a relaxation taking place in the 0.6–1.8 ps time range after CO photodissociation. Mb and FixLH have different heme transient structures at $\Delta t = +1$ ps after diatomic dissociation, which are not that of steady-state deoxy forms. For FixL, we found

that the heme structure imposed in the bound state and the primary intermolecular interaction after dissociation depends on the nature of the ligand.

Supporting information

Supporting information may be found in the online version of this article.

References

[1] J. W. Petrich, C. Poyart, J. L. Martin, *Biochemistry* **1988**, *27*, 4049.
[2] Y. Kholodenko, E. A. Gooding, Y. Dou, M. Ikeda-Saito, R. M. Hochstrasser, *Biochemistry* **1999**, *38*, 5918.
[3] D. Ionascu, F. Gruia, X. Ye, A. C. Yu, F. Rosca, C. Beck, A. Demidov, J. S. Olson, P. M. Champion, *J. Am. Chem. Soc.* **2005**, *127*, 16921.
[4] C. Gautier, M. Negrerie, Z. Q. Wang, J. C. Lambry, D. J. Stuehr, F. Collin, J. L. Martin, A. Slama-Schwok, *J. Biol. Chem.* **2004**, *279*, 4358.
[5] M. Negrerie, L. Bouzhir, J. L. Martin, U. Liebl, *J. Biol. Chem.* **2001**, *276*, 46815.
[6] U. Liebl, L. Bouzhir-Sima, L. Kiger, M. C. Marden, J. C. Lambry, M. Negrerie, M. H. Vos, *Biochemistry* **2003**, *42*, 6527.
[7] M. H. Lim, T. A. Jackson, P. A. Anfinrud, *Nat. Struct. Biol.* **1997**, *4*, 209.
[8] S. Kim, G. Jin, M. H. Lim, *J. Phys. Chem. B* **2004**, *108*, 20366.
[9] S. Kim, M. Lim, *J. Am. Chem. Soc.* **2005**, *127*, 8908.
[10] J. Treuffet, K. J. Kubarych, J. C. Lambry, E. Pilet, J. B. Masson, J. L. Martin, M. H. Vos, M. Joffre, A. Alexandrou, *Proc. Nat. Acad. Sci. U.S.A.* **2007**, *104*, 15705.

[11] A. Rupenyan, J. Commandeur, M. L. Groot, *Biochemistry* **2009**, *48*, 6104.

[12] E. W. Findsen, J. M. Friedman, M. R. Ondrias, S. R. Simon, *Science* **1985**, *229*, 661.

[13] E. W. Findsen, T. W. Scott, M. R. Chance, J. M. Friedman, M. R. Ondrias, *J. Am. Chem. Soc.* **1985**, *107*, 3355.

[14] J. W. Petrich, J. L. Martin, D. Houde, C. Poyart, A. Orszag, *Biochemistry* **1987**, *26*, 7914.

[15] J. W. Petrich, J. L. Martin, *Chem. Phys.* **1989**, *131*, 31.

[16] S. Franzen, J. C. Lambry, B. Bohn, C. Poyart, J. L. Martin, *Nat. Struct. Biol.* **1994**, *1*, 230.

[17] S. Franzen, B. Bohn, C. Poyart, J. L. Martin, *Biochemistry* **1995**, *34*, 1224.

[18] Y. Mizutani, T. Kitagawa, *J. Phys. Chem. B* **2001**, *105*, 10992.

[19] A. Sato, Y. Sasakura, S. Sugiyama, I. Sagami, T. Shimizu, Y. Mizutani, T. Kitagawa, *J. Biol. Chem.* **2002**, *277*, 32650.

[20] S. Cianetti, M. Negrerie, M. H. Vos, J. L. Martin, S. G. Kruglik, *J. Am. Chem. Soc.* **2004**, *126*, 13932.

[21] S. Cianetti, S. G. Kruglik, M. H. Vos, P. Y. Turpin, J. L. Martin, M. Negrerie, *Biochim. Biophys. Acta* **2004**, *1658*(Suppl. 1), 218.

[22] M. Negrerie, S. Cianetti, M. H. Vos, J. L. Martin, S. G. Kruglik, *J. Phys. Chem. B.* **2006**, *110*, 12766.

[23] M. Negrerie, S. G. Kruglik, J. C. Lambry, M. H. Vos, J. L. Martin, S. Franzen, *J. Biol. Chem.* **2006**, *281*, 10389.

[24] S. G. Kruglik, J. C. Lambry, S. Cianetti, J. L. Martin, R. R. Eady, C. R. Andrew, M. Negrerie, *J. Biol. Chem.* **2007**, *282*, 5062.

[25] S. G. Kruglik, A. Jasaitis, K. Hola, T. Yamashita, U. Liebl, J. L. Martin, M. H. Vos, *Proc. Nat. Acad. Sci. U.S.A.* **2007**, *104*, 7408.

[26] T. Kitagawa, in *Biological Applications of Raman Spectroscopy*, vol. 3 (Ed.: T. G. Spiro) Wiley: New York, **1988**, pp 97.

[27] T. G. Spiro, X. Y. Li, in *Biological Applications of Raman Spectroscopy*, vol. 3 (Ed.: T. G. Spiro), Wiley: New York, **1988**, pp 1.

[28] R. Lingle, X. B. Xu, H. Zhu, S.-C. Yu, J. B. Hopkins, K. D. Straub, *J. Am. Chem. Soc.* **1991**, *113*, 3992.

[29] P. Li, J. T. Sage, P. M. Champion, *J. Chem. Phys.* **1992**, *97*, 3214.

[30] V. Jayaraman, K. R. Rodgers, I. Mukerji, T. G. Spiro, *Science* **1995**, *269*, 1843.

[31] Y. Mizutani, T. Kitagawa, *Science* **1997**, *278*, 443.

[32] S. G. Kruglik, Y. Mizutani, T. Kitagawa, *Chem. Phys. Lett.* **1997**, *266*, 283.

[33] S. G. Kruglik, P. Mojzes, Y. Mizutani, T. Kitagawa, P. Y. Turpin, *J. Phys. Chem. B* **2001**, *105*, 5018.

[34] A. Sato, Y. Gao, T. Kitagawa, Y. Mizutani, *Proc. Nat. Acad. Sci. U.S.A.* **2007**, *104*, 9627.

[35] H. Hamaguchi, T. L. Gustafson, *Annu. Rev. Phys. Chem.* **1994**, *45*, 593.

[36] K. Iwata, S. Yamaguchi, H. Hamaguchi, *Rev. Sci. Instrum.* **1993**, *64*, 2140.

[37] R. M. Butler, M. A. Lynn, T. L. Gustafson, *J. Phys. Chem.* **1993**, *97*, 2609.

[38] Y. Uesugi, Y. Mizutani, T. Kitagawa, *Rev. Sci. Instrum.* **1997**, *68*, 4001.

[39] L. Zhu, J. Kim, R. A. Mathies, *J. Raman Spectrosc.* **1999**, *30*, 777.

[40] Y. Uesugi, Y. Mizutani, S. G. Kruglik, A. G. Shvedko, V. A. Orlovich, T. Kitagawa, *J. Raman Spectrosc.* **2000**, *31*, 339.

[41] M. Towrie, A. W. Parker, W. Shaikh, P. Matousek, *Meas. Sci. Technol.* **1998**, *9*, 816.

[42] W. Henry, C. G. Coates, C. Brady, K. L. Ronayne, P. Matousek, M. Towrie, S. W. Botchway, A. W. Parker, J. G. Vos, W. R. Browne, J. J. McGarvey, *J. Phys. Chem. A* **2008**, *112*, 4537.

[43] A. Vlcek, I. R. Farrell, D. J. Liard, P. Matousek, M. Towrie, A. W. Parker, D. C. Grills, M. W. George, *J. Chem. Soc., Dalton Trans.* **2002**, *5*, 701.

[44] M. Mizuno, S. Yamaguchi, T. Tahara, *J. Phys. Chem. A* **2005**, *109*, 5257.

[45] D. W. McCamant, P. Kukura, S. Yoon, R. A. Mathies, *Rev. Sci. Instrum.* **2004**, *75*, 4971.

[46] Z. Sun, J. Lu, D. H. Zhang, and S. Y. Lee, *J. Chem. Phys.* **2008**, *128*, 144114.

[47] S. Yoon, D. W. McCamant, P. Kukura, R. A. Mathies, D. Zhang, S. Y. Lee, *J. Chem. Phys.* **2005**, *122*, 024505.

[48] S. Y. Lee, D. Zhang, D. W. McCamant, P. Kukura, R. A. Mathies, *J. Chem. Phys.* **2004**, *121*, 3236.

[49] D. W. McCamant, P. Kukura, R. A. Mathies, *J. Phys. Chem. A* **2003**, *107*, 8208.

[50] P. Kukura, D. W. McCamant, S. Yoon, D. B. Wandschneider, R. A. Mathies, *Science* **2005**, *310*, 1006.

[51] W. Kiefer, A. Materny, M. Schmitt, *Naturwiss* **2002**, *89*, 250.

[52] B. D. Prince, A. Chakraborty, B. M. Prince, H. U. Stauffer, *J. Chem. Phys.* **2006**, *125*, 044502.

[53] L. Zhu, W. Wang, J. T. Sage, P. M. Champion, *J. Raman Spectrosc.* **1995**, *26*, 527.

[54] L. Zhu, J. T. Sage, P. M. Champion, *Science* **1994**, *266*, 629.

[55] M. Kubo, F. Gruia, A. Bennabbas, A. Barabanschikov, W. R. Montfort, E. M. Maes, P. M. Champion, *J. Am. Chem. Soc.* **2008**, *130*, 9800.

[56] A. Bonvalet, M. Joffre, J. L. Martin, A. Migus, *Appl. Phys. Lett.* **1995**, *67*, 2907.

[57] J. Rodriguez, C. Kirmaier, D. Holten, *J. Am. Chem. Soc.* **1989**, *111*, 6500.

[58] U. Liebl, L. Bouzhir-Sima, M. Negrerie, J. L. Martin, M. H. Vos, *Proc. Nat. Acad. Sci. U.S.A.* **2002**, *99*, 12771.

[59] S. Sato, K. Kamogawa, K. Aoyagi, T. Kitagawa, *J. Phys. Chem.* **1992**, *96*, 10676.

[60] S. Hu, K. M. Smith, T. G. Spiro, *J. Am. Chem. Soc.* **1996**, *118*, 12638.

[61] A. Desbois, M. Lutz, R. Banerjee, *Biochemistry* **1979**, *18*, 1510.

[62] R. E. Hester, P. Matousek, J. N. Moore, A. W. Parker, W. T. Toner, M. Towrie, *Phys. Chem. Lett.* **1993**, *208*, 471.

[63] K. Iwata, H. Hamaguchi, *Phys. Chem. A* **1997**, *101*, 632.

[64] X. Ye, A. Demidov, F. Rosca, W. Wang, A. Kumar, D. Ionascu, L. Zhu, D. Barrick, D. Wharton, P. M. Champion, *J. Phys. Chem. A* **2003**, *107*, 8156.

[65] T. Tomita, G. Gonzalez, A. L. Chang, M. Ikeda-Saito, M. A. Gilles-Gonzalez, *Biochemistry* **2002**, *41*, 4819.